Experimental measurements of a betatron difference resonance

M. Ellison,[1] M. Ball,[1] B. Brabson,[1] J. Budnick,[1] D.D. Caussyn,[1] A.W. Chao,[2] V. Derenchuk,[1] S. Dutt,[2] G. East,[1] D. Friesel,[1] B. Hamilton,[1] H. Huang,[1] W.P. Jones,[1] S.Y. Lee,[1] D. Li,[1] M.G. Minty,[3] K.Y. Ng,[4] X. Pei,[1] A. Riabko,[1] T. Sloan,[1] M. Syphers,[2] Y. Wang,[1] Y. Yan,[2] and P.L. Zhang[2]

[1]*Indiana University Cyclotron Facility, Indiana University, Bloomington, Indiana 47405*

[2]*The Superconducting Super Collider Laboratory, 2550 Beckleymeade Avenue, Dallas, Texas 75237-3946*

[3]*Stanford Linear Accelerator Center, MS26, Box 4349, Stanford, California 94309*

[4]*Fermilab, P.O. Box 500, Batavia, Illinois 60510*

(Received 24 May 1994)

The betatron difference resonance, $Q_x - 2Q_z = -6$, where the $Q_{x,z}$ are the number of betatron oscillations per revolution, was studied at the Indiana University Cyclotron Facility cooler ring. Measurements of both vertical and horizontal coherent betatron oscillations were made, at a nonlinear resonance, after a pulsed dipole kick. We found that the Poincaré surface of section for the nonlinear resonance could be described by a simple Hamiltonian. The resonance strength and phase, as well as the tune shift, as a function of betatron amplitude, were deduced from the experimental data. Attempts to deduce the amplitude and phase of the time dependent fluctuations around the time averaged Poincaré surface of section will also be discussed.

PACS number(s): 29.27.Bd, 41.75.−i, 03.20.+i, 05.45.+b

I. INTRODUCTION

Modern storage rings routinely store particles for 10^{10} revolutions. In order to prevent luminosity degradation over these "cosmic" time scales, the mechanisms that cause the amplitude of the transverse oscillations to increase, must be understood. One such mechanism, which is related to the nonlinearities in the magnetic fields, has attracted considerable interest. Of particular interest have been the magnetic field errors in the superconducting magnets as the magnetic field strength is pushed to the limit.

Several methods have been developed to study the nonlinear dynamics of circular accelerators analytically. These methods include the Lie algebraic method [1], perturbation techniques [2,3], and the differential algebraic method [4,5]. These works have led to important advances in nonlinear beam dynamics. These studies highlighted the detrimental effects of resonant conditions on the luminosity and the beam lifetime. For example, a strong isolated resonance can cause rapid amplitude growth and overlapping resonances in phase space can lead to stochastic motion.

Experimental studies [6–10] of resonant behavior are useful in determining the validity and limitations of the approximations used in the computational studies. The majority of these experiments studied particle motion near a one-dimensional (1D) betatron resonance. Since the resonances that drive the growth in amplitude of betatron oscillations are often two dimensional (2D), experimental measurements of 2D resonances are called for. The effort to observe the effects from a 2D resonance experimentally has achieved only limited success [10]. The main difficulty that experimenters have faced is the rapid decoherence of the coherently kicked bunch. The experiment reported in Ref. [10], for example, was greatly hindered by the rapid decoherence inherent in an electron machine. In order to determine a 2D nonlinear Hamiltonian unambiguously, the invariant surface of the 2D resonance should be reconstructed. Towards this goal, the cooler ring at the Indiana University Cyclotron Facility (IUCF) has a natural advantage [11]. The IUCF cooler ring has an electron cooling system which can reduce both the transverse and longitudinal emittance of the proton beam to small values. The 95% transverse emittance can be cooled to 0.3 (πmm mrad) in about 1 s while the 95% longitudinal phase space area can be cooled to about 2×10^{-4} eV s. A beam with such a small emittance can closely simulate single particle motion in a synchrotron. Our previous experiments [7–9,12] have clearly demonstrated this advantage.

This paper details a two-dimensional experimental tracking of particle motion near a nonlinear resonance condition in a proton machine. Section II gives a brief overview of the derivation of the Hamiltonian assuming sextupole nonlinearities. Section III details how the Hamiltonian for the cooler ring was empirically determined, and highlights the correspondence between the theoretical predictions of the simple Hamiltonian analysis and the experimental observations. Attempts to deduce the time dependent terms in the Hamiltonian will also be addressed in this section. Section IV compares the values of the resonance strength and its phase to the values predicted from the known sextupole nonlinearities. The conclusion is given in Sec. V.

II. THE HAMILTONIAN OF THE NONLINEAR RESONANCE

For particle motion in a circular accelerator, the horizontal and vertical deviations from the closed orbit $x(s)$

and $z(s)$ in the presence of magnetic field errors $\Delta B_{x,z}$ are given by Hill's equation

$$\frac{d^2x}{ds^2} + K_x(s)x = \frac{\Delta B_z(s)}{B\rho}, \quad \frac{d^2z}{ds^2} + K_z(s)z = -\frac{\Delta B_x(s)}{B\rho}, \tag{1}$$

with

$$\Delta B_z + i\Delta B_x = \sum_{n\geq 2}(b_n + ia_n)(x+iz)^n,$$

where b_n and a_n are the normal and the skew multipole components, respectively. The focusing functions are given by $K_x(s) = \frac{1}{\rho^2} - \frac{B'}{B\rho}$ and $K_z(s) = \frac{B'}{B\rho}$ where $B' = \frac{dB_z}{dx}$, $B\rho$ is the magnetic rigidity, and s is the longitudinal particle coordinate which advances from 0 to C, the circumference, as the particle completes one revolution. Hereafter, the subscript y designates either the x or z plane. Both $K_y(s)$ and the field error term $\Delta B_y(s)/B\rho$ are periodic functions of s with period C.

For a linear machine, for which $\Delta B_y(s) = 0$, a solution to Hill's equation exists [13], which constitutes a pseudo-harmonic oscillation

$$y = \sqrt{2\beta_y(s)J_y}\cos(\phi_y + \psi_y), \tag{2}$$

where β_y is the betatron amplitude function, (J_y, ϕ_y) are the conjugate action-angle variables, $\psi_y(s) = \int_{s_o}^{s}\frac{ds}{\beta_y} - Q_y\theta$ is the "flutter" of the betatron phase with the tune $Q_y = \frac{1}{2\pi}\oint\frac{ds}{\beta_y}$ as the number of betatron oscillations in one revolution, and $\theta = s/R$ as the orbital angle where R is the average radius of the accelerator.

Since we are studying the $Q_x - 2Q_z = -6$ resonance, we will only consider the Hamiltonian for an accelerator with sextupole nonlinearities. After the transformation to the action-angle variables outlined above and with θ being the independent or "time" variable, the Hamiltonian is given by

$$H = Q_xI_x + Q_zI_z + \sum_j\Big[(2I_x\beta_x)^{3/2}\left(\frac{B''l}{6B\rho}\right) \times\cos^3(\phi_x+\psi_x) - (2I_x\beta_x)^{1/2}(2I_z\beta_z)\left(\frac{B''l}{2B\rho}\right) \times\cos(\phi_x+\psi_x)\cos^2(\phi_z+\psi_z)\Big]\delta(\theta-\theta_j), \tag{3}$$

where the sum over j contains all the sextupole fields in the accelerator, $B'' = d^2B_z/dx^2$, and l is the length of the sextupole. The nonlinear perturbation term can be expanded into a Fourier series, and the Hamiltonian becomes [2]

$$\begin{aligned} H = {} & Q_xI_x + Q_zI_z + (2I_x)^{3/2}\sum_m[A_{30m}\cos(3\phi_x - m\theta + \alpha_{30m}) + 3A_{10m}\cos(\phi_x - m\theta + \alpha_{10m})] \\ & -(2I_x)^{1/2}(2I_z)\sum_m[B_{12m}\cos(\phi_x + 2\phi_z - m\theta + \beta_{12m}) \\ & + B_{1-2m}\cos(\phi_x - 2\phi_z - m\theta + \beta_{1-2m}) + 2B_{10m}\cos(\phi_x - m\theta + \beta_{10m})] \end{aligned} \tag{4}$$

where the sum over m extends from $-\infty$ to $+\infty$ with

$$A_{30m}e^{i\alpha_{30m}} = \sum_j S_je^{(3\psi_x+m\theta)_j}, \quad A_{10m}e^{i\alpha_{10m}} = \sum_j S_je^{(\psi_x+m\theta)_j},$$

$$B_{1\pm2m}e^{i\beta_{1\pm2m}} = \sum_j W_je^{(\psi_x\pm2\psi_z+m\theta)_j}, \quad B_{10m}e^{i\beta_{10m}} = \sum_j W_je^{(\psi_x+m\theta)_j},$$

$$S_j = \frac{B''l}{48\pi B\rho}\beta_x^{3/2}, \quad W_j = \frac{B''l}{16\pi B\rho}\beta_x^{1/2}\beta_z. \tag{5}$$

Here the harmonic amplitudes A_{ijk},B_{ijk} and the phases α_{ijk},β_{ijk} are real numbers.

We can remove the time dependence from the Hamiltonian, to first order in the strength of the perturbation, by a canonical transformation with the generating function

$$G_1(\phi_x, J_x, \phi_z, J_z; \theta) = \phi_xJ_x + \phi_zJ_z - (2J_x)^{3/2}\Sigma_a + (2J_x)^{1/2}(2J_z)\Sigma_b, \tag{6}$$

where

$$\begin{aligned} \Sigma_a &= \sum_m[f_{10m}\sin(\phi_x - m\theta + \alpha_{1m}) + f_{30m}\sin(3\phi_x - m\theta + \alpha_{3m})], \\ \Sigma_b &= \sum_m[F_{12m}\sin(\phi_x + 2\phi_z - m\theta + \beta_{12m}) + F_{1-2m}\sin(\phi_x - 2\phi_z - m\theta + \beta_{1-2m}) + F_{10m}\sin(\phi_x - m\theta + \beta_{1m})]. \end{aligned} \tag{7}$$

The new action-angle variables become

$$I_x = \frac{\partial G_1}{\partial \phi_x} = J_x - (2J_x)^{3/2}\frac{\partial \Sigma_a}{\partial \phi_x} + (2J_x)^{1/2}(2J_z)\frac{\partial \Sigma_b}{\partial \phi_x}, \quad I_z = \frac{\partial G_1}{\partial \phi_z} = J_z + (2J_x)^{1/2}(2J_z)\frac{\partial \Sigma_b}{\partial \phi_z},$$
$$\gamma_x = \frac{\partial G_1}{\partial J_x} = \phi_x - 3(2J_x)^{1/2}\Sigma_a + (2J_x)^{-1/2}(2J_z)\Sigma_b, \quad \gamma_z = \frac{\partial G_1}{\partial J_z} = \phi_z + 2(2J_x)^{1/2}\Sigma_b. \tag{8}$$

Writing the old Hamiltonian in terms of the new action-angle variables, expanding it in a Taylor series, and retaining terms up to second order in the strength of the perturbation, the new Hamiltonian becomes

$$\begin{aligned} H_1 = H + \frac{\partial G_1}{\partial \theta} \approx\ & Q_x J_x + Q_z J_z + \frac{A_{xx}}{2}J_x^2 + A_{xz}J_xJ_z + \frac{A_{zz}}{2}J_z^2 \\ & + (2J_x)^{3/2}\sum_m \Big[[A_{30m} - f_{30m}(3Q_x - m)]\cos(3\phi_x - m\theta + \alpha_{30m}) + [3A_{10m} - f_{10m}(Q_x - m)]\cos(\phi_x - m\theta + \alpha_{10m})\Big] \\ & - (2J_x)^{1/2}(2J_z)\sum_m \Big[[B_{12m} - F_{12m}(Q_x + 2Q_z - m)]\cos(\phi_x + 2\phi_z - m\theta + \beta_{12m}) \\ & + [B_{1-2m} - F_{1-2m}(Q_x - 2Q_z - m)]\cos(\phi_x - 2\phi_z - m\theta + \beta_{1-2m}) \\ & + [2B_{10m} - F_{10m}(Q_x - m)]\cos(\phi_x - m\theta + \beta_{10m})\Big], \end{aligned} \tag{9}$$

where A_{ij} are both θ dependent and second order in sextupole strength. Finally, by appropriately choosing the F_{klm}, f_{klm},

$$f_{10m} = \frac{3A_{10m}}{Q_x - m}, \quad f_{30m} = \frac{A_{30m}}{3Q_x - m},$$
$$F_{1\pm 2m} = \frac{B_{1\pm 2m}}{Q_x \pm 2Q_z - m}, \quad F_{10m} = \frac{2B_{10m}}{Q_x - m}, \tag{10}$$

we obtain a Hamiltonian with new action-angle variables, Eq. (8), where the new actions J_x and J_z are, to first order in the sextupole strength, constants of motion.

Note here that (γ_x, J_x) and (γ_z, J_z) are new conjugate phase space coordinates. However, the betatron phase angle coordinate γ_y can be approximated by ϕ_y. Approximating γ_y by ϕ_y is allowable since we only keep terms up to second order in the strength of the perturbation and

$$\cos\left(f(\gamma_y)\right) = \cos\left(f(\phi_y) + O(\epsilon)\right) \approx \cos\left(f(\phi_y)\right) + O(\epsilon), \tag{11}$$

where ϵ represents the sextupole strength. Thus we will use (ϕ_y, J_y) as the conjugate phase space coordinates.

Experimentally, we measure ϕ_y and I_y, the action-angle variables (γ_y, J_y) after the canonical transformation can be obtained from the filtering method, i.e., $\gamma_y = \langle \phi_y \rangle$ and $J_y = \langle I_y \rangle$. In some of our data analysis, a 10-revolution average method was applied to filter the time dependent terms.

Note that the canonical perturbation diverges when a particular resonance is encountered. Thus, when the betatron tune is close to a resonance, that particular harmonic cannot be treated perturbatively. For example, when the betatron tunes are near the $Q_x - 2Q_z = -6$ resonance, we can perform a canonical transformation for all F_{klm}, f_{klm} except F_{1-2-6}. Transforming all the harmonics except F_{1-2-6}, the Hamiltonian of Eq. (9), including the sextupole perturbation, can then be written as

$$\begin{aligned} H_1 = {} & Q_x J_x + Q_z J_z + \frac{\alpha_{xx}}{2}J_x^2 + \alpha_{xz}J_xJ_z + \frac{\alpha_{zz}}{2}J_z^2 \\ & + 2^{3/2}BJ_x^{1/2}J_z\cos(\phi_x - 2\phi_z + 6\theta + \mu), \end{aligned} \tag{12}$$

where the detuning parameters α_{ij} are the average of the A_{ij} found in Eq. (9) over θ in one complete revolution (see Appendix A), $B = B_{1-2-6}$ and $\mu = \beta_{1-2-6}$.

The Hamiltonian of Eq. (12) will be used to describe particle motion near the single dominant resonance $Q_x - 2Q_z = -6$. This Hamiltonian can be transformed to a time independent form by performing one further canonical transformation into a "rotating reference frame" with the generating function

$$G_2(\phi_x, \phi_z, J_1, J_2) = J_1(\phi_x - 2\phi_z + 6\theta + \mu) + J_2\phi_z. \tag{13}$$

The new coordinates are, $\phi_1 = \phi_x - 2\phi_z + 6\theta + \mu$, $\phi_2 = \phi_z$, $J_1 = J_x$, and $J_2 = J_z + 2J_x$. This new Hamiltonian becomes

$$\begin{aligned} H_2 = {} & \delta_1 J_1 + \frac{\alpha_{11}}{2}J_1^2 + 2^{3/2}BJ_1^{1/2}(J_2 - 2J_1)\cos\phi_1 \\ & + \left[Q_zJ_2 + \frac{\alpha_{zz}}{2}J_2^2\right], \end{aligned} \tag{14}$$

where the resonance proximity parameter is

$$\delta_1 = Q_x - 2Q_z + 6 + (\alpha_{xz} - 2\alpha_{zz})J_2, \tag{15}$$

and the effective nonlinear detuning parameter is $\alpha_{11} = \alpha_{xx} - 4\alpha_{xz} + 4\alpha_{zz}$. This new Hamiltonian is independent of θ and ϕ_2, thus H_2 and J_2 are constants of motion which determine the particle motion completely. Hamilton's equations of motion are given by

$$\dot{J} = 2^{3/2}BJ_1^{1/2}(J_2 - 2J_1)\sin\phi_1, \tag{16}$$
$$\dot{\phi}_1 = \delta_1 + \alpha_{11}J_1 + 2^{1/2}BJ_1^{-1/2}(J_2 - 6J_1)\cos\phi_1. \tag{17}$$

The stable and unstable fixed points (SFP and UFP, respectively) are given by the solutions of

$$\delta_1 J_{1,\mathrm{FP}}^{1/2} + \alpha_{11}J_{1,\mathrm{FP}}^{3/2} \pm 2^{1/2}B(J_2 - 6J_{1,\mathrm{FP}}) = 0, \tag{18}$$

where the + and − signs correspond to $\phi_{1,\mathrm{FP}} = 0$ and π, respectively. For this 2D resonance, there are two additional unstable fixed points located at

$$(J_{1,\mathrm{UFP}}, \phi_{1,\mathrm{UFP}}) = \left(\frac{J_2}{2}, \pm \arccos \left[\frac{2\delta_1 + \alpha_{11} J_2}{8 B J_2^{1/2}} \right] \right). \tag{19}$$

The Hamiltonian flow for a particle with the initial conditions $J_{z0} = 0$, and $J_2 = 2J_{x0}$, is given by

$$(2J_1 - J_2)\left[\frac{\alpha_{11}}{4} J_1 - 2^{3/2} B J_1^{1/2} \cos\phi_1 + \frac{\delta_1}{2} + \frac{\alpha_{11}}{8} J_2 \right] = 0. \tag{20}$$

Here, the particle trajectory follows the path of two circles in the map of

$$(\sqrt{2\beta_x J_1}\cos\phi_1, \sqrt{2\beta_x J_1}\sin\phi_1).$$

If these two circles intersect, the circle $2J_1 = J_2$ can be dissected by an arc of the circle describing the nonlinear coupling (see Appendix B). The circle $2J_1 = J_2$ is called the "launching" circle, while the circle

$$\frac{\alpha_{11}}{4} J_1 - 2^{3/2} B J_1^{1/2} \cos\phi_1 + \frac{\delta_1}{2} + \frac{\alpha_{11}}{8} J_2 = 0 \tag{21}$$

is the nonlinear "coupling" circle. The intersection of these two circles are the UFP's of Eq. (19), where the launching circle and the coupling arc form a separatrix orbit of the Hamiltonian flow.

Thus, the particle motion near a 2D resonance can be transformed to an invariant surface which is described by the intersection of two circles. Matching the measured particle trajectories with the contours of constant H_2, we can determine B, α_{11}, and δ_1 up to an arbitrary multiplicative constant. One parameter must be known independently for the scale to be fixed and H_2 uniquely determined. The method by which this was accomplished is described in the next section.

Since Hamiltonian tori cannot cross each other, particles with identical δ_1 and J_2, will form nonintersecting tori around the stable fixed points limited by the launching circle $2J_1 = J_2$ and the coupling arc. For particles with different δ_1 and/or J_2, the coupling circle is translated along the horizontal axis in the phase space of the resonance rotating frame with different radius of curvature (see Appendix B).

III. EXPERIMENTAL METHOD AND DATA AND ANALYSIS

A. Experimental method

Protons were injected into the IUCF cooler ring at 45 MeV on a 10 s timing cycle. The beam was bunched at harmonic number $h = 1$, with the rf cavity operating at 1.031 68 MHz. The bunched beam was electron cooled for 3 s reducing its 95% emittance to less than 0.3 (π mm mrad). The motion of a beam bunch with such a small emittance has been observed to remain coherent for 10^4 revolutions.

The linear coupling resonance was found to be important in our previous studies [7,8], it was first corrected by using a pair of skew quadrupoles. To study the 2D betatron difference resonance the betatron tunes were adjusted to be near the resonance line $Q_x - 2Q_z = -6$. Although the dynamical aperture was slightly smaller, it was possible to store the beam with the betatron tunes on the difference resonance since $J_2 = J_z + 2J_x$ is invariant. Thus, the resonance did not cause excessive beam loss since the action in both planes of oscillation was bounded.

A coherent transverse oscillation was imparted to the bunch by firing single-turn pulsed kicker magnets. The subsequent coherent betatron motion was obtained from signals from the beam position monitors (BPM), where the betatron amplitude functions were measured to be $\beta_{x1} = 10.2$ m, $\beta_{x2} = 7.4$ m, $\beta_{z1} = 14.1$ m, and $\beta_{z2} = 14.0$ m, respectively. These transverse betatron oscillations were recorded on a turn-by-turn basis [9] for a complete grid of horizontal and vertical kicker strengths. The gain of the data acquisition system was calibrated against the beam position monitoring system in the cooler ring which itself was calibrated against a wire scanner. The uncertainty in position gain is estimated to be ±10%. The rms position of the BPM system was found to be about 0.1 mm. The conversion from two position measurements (y_1, y_2) in each plane to normalized position and momentum coordinates (y, P_y), where $P_y = -\sqrt{2\beta_y J_y}\sin(\phi + \psi_y)$ is the conjugate momentum variable to the coordinate of Eq. (2), have been described in some detail in a previous paper [9].

B. Data reduction

An example of the raw data is shown in Fig. 1 which displays the position measured at each revolution in both the horizontal and the vertical planes of oscillation as a horizontal kick occurred. The particular characteristics of the betatron oscillations near a nonlinear resonance are clearly visible in Fig. 1, where the off-phase amplitude oscillation arises from the fact that J_2 is a constant of motion and the sharp rise in vertical amplitude is due to a nonlinear dependence in the Hill's equation. The fast Fourier transform (FFT) of the position measurements are also displayed in Fig. 1, where the sidebands resulting from the nonlinear coupling are evident. The two position measurements, in each plane of oscillation, were first converted to the normalized coordinates. The top two plots in Fig. 2 display the Poincaré maps in (x, P_x) and (z, P_z) of the same kick shown in Fig. 1, where the smear in the Poincaré maps is due to the nonlinear coupling. Then the phase space coordinates ϕ_x, ϕ_z, $J_x \approx I_x$ and $J_z \approx I_z$ were computed for each revolution from the normalized Poincaré map. The resonance phase ϕ_1 can then be derived. The bottom plot in Fig. 2 shows the Poincaré map in the resonant precessing frame derived from the data in the top two plots, where the phase μ of Eq. (13) was determined to be $\mu = \mu_m = -2.13$ rad so that the coupling line is adjusted to the upright position.

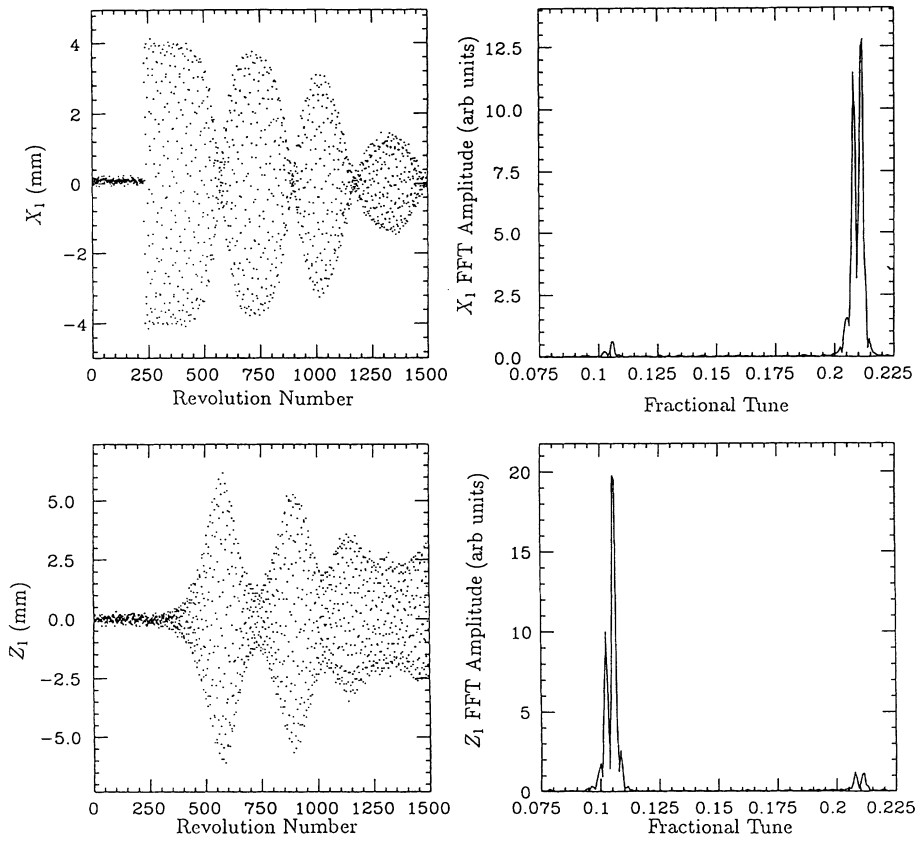

FIG. 1. Plot of the measured positions at each revolution in both the horizontal and the vertical planes of oscillation as a horizontal kick occurred. The FFT's of the position measurements are also displayed. The sidebands resulting from the nonlinear coupling are evident.

Since the data set displayed in the lower plot of Fig. 2 was obtained solely from an initial horizontal kick, there was no coherent motion from which ϕ_z could be measured. The resulting data points in the Poincaré surface of section were observed to fill the entire launching circle. When some of the action was coupled into the vertical betatron plane so that ϕ_z could be measured, the measurement of ϕ_1 first stabilized, as expected, at the intersection of the launching and coupling circles. The data then traced several loops around the coupling arc and the right side of the launching circle until the kick finally decohered.

1. *Measurement of the detuning parameters*

It was thought that measurements of the tune shift with amplitude parameters α_{ij} could be made directly. With α_{11} known, H_2 could then be uniquely determined. To measure the α parameters, one needs only to find the slope of the betatron tunes vs the betatron actions. However, our measurements were complicated by two factors. First, the resonance stop band was larger than anticipated so that even with $|Q_x - 2Q_z + 6| > 0.05$ the effect of the resonance was evident, which complicated the measurement of the detuning parameters. Second, the unperturbed betatron tunes of the cooler ring are not stable.

Since our BPM system has position resolution of about 0.1 mm, one can measure the tune, assuming a pure tone, to better than $\pm\ 1 \times 10^{-4}$ by tracking and averaging the phase in (y, P_y) phase space over 50 turns for coherent betatron oscillations larger than 1 mm. Using this tune tracking method, we observed a tune modulation in Q_x of ± 0.0005 and in Q_z of ± 0.002. An example of this tune modulation is shown in Fig. 3 where the amplitude of the tune modulation is about 0.002. The frequency components of the tune modulation are harmonics of 60 Hz. Since the expected nonlinear detuning is of the same order of magnitude, it is difficult to measure the nonlinear detuning coefficients.

2. *Measurement of the detuning parameters using a "two-kick" method*

Due to a power supply ripple, it was not possible to measure the nonlinear detuning parameters α_{ij} by measuring the betatron tunes as a function of the betatron oscillation amplitude. However, it was later found that a two-kick procedure allowed for the measurement of the α parameters even when the base tunes were not stable. Since there was only one vertical kicker available in the IUCF Cooler Ring, the two-kick method was made possible by first using the rf knockout system and then followed by a coherent vertical kick. This method is actually used for both horizontal and vertical planes.

The bunch was first given a small coherent oscillation by applying an rf voltage, at a betatron sideband frequency, to a transverse BPM. This knockout imparted

a coherent transverse oscillation to the beam, which allowed the phase of the betatron oscillation to be tracked and thus, the base tune to be measured. The bunch was then given a larger kick with one of the pulsed kicker magnets 500 revolutions later. In this way the tune change resulting from the change in betatron actions could be accurately measured.

The results of this procedure are shown in Fig. 4, where both the position and tune measurement are plotted. By inspecting both Fig. 3 and Fig. 4 one observes that the change in tune due to the change in action, is small compared to the change in tune resulting from the power supply ripple. The α parameters were measured using the two-kick procedure when $Q_x - 2Q_z + 6 \approx -0.08$ in a different run. The fact that the value of $\alpha_{11} = -455\ (\pi\mathrm{m})^{-1}$, determined at this tune location, differed from the value of $\alpha_{11} = 2100\ (\pi\mathrm{m})^{-1}$ (see Sec. III C), determined from the resonance data, is not surprising. This is because the detuning from sextupoles is a second order effect and so depends sensitively on the betatron phase advance between sextupoles in the cooler ring. Nevertheless, the technique of using two kicks will be useful in improving the correspondence between the measured and the calculated values of the resonance strengths and detuning parameters in the future.

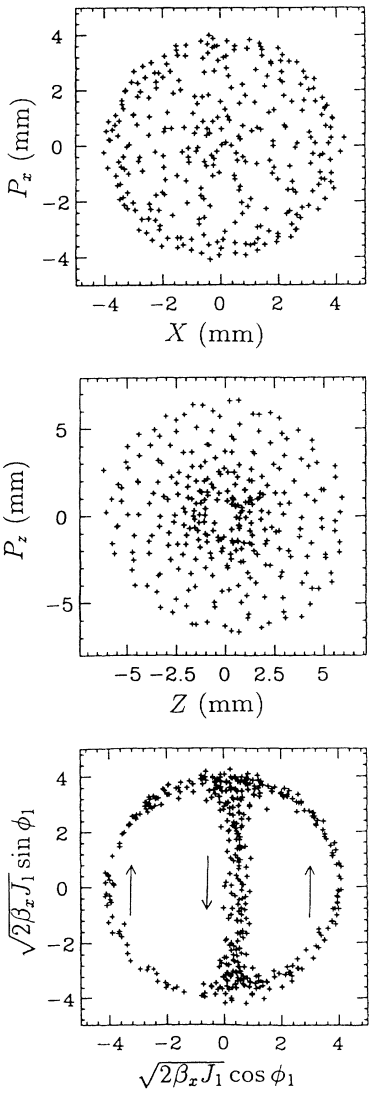

FIG. 2. The top two plots display the Poincaré maps in (x, P_x),(z, P_z) of the same kick shown in Fig. 1. The bottom plot in Fig. 2 displays the Poincaré surface of section in the resonant precessing frame derived from the data in the top two plots. The resonance phase μ of Eq. (12) was determined to be -2.13 rad so that the coupling arc is in the upright position.

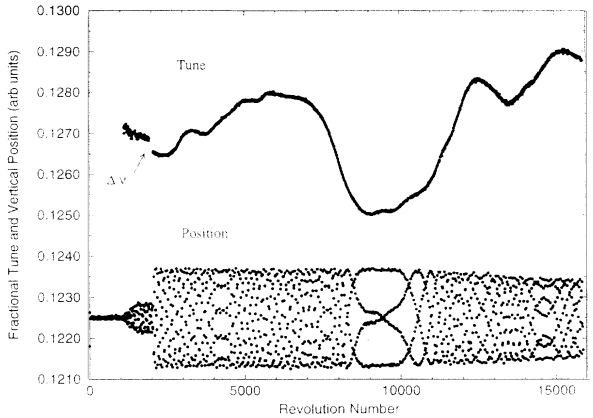

FIG. 3. Plot, at 10 revolution intervals, of both the measured vertical fractional tune ν_z and the position measurement at the first vertical BPM vs revolution number. The discontinuity near revolution number 2000 is explained in Sec. III B 1. Until coherent motion develops in the vertical plane, which occurs at about revolution number 1200, it is not possible to measure the vertical fractional tune. The variation in the tune ν_z is about $\pm$ 0.002 which is probably due to a power supply ripple.

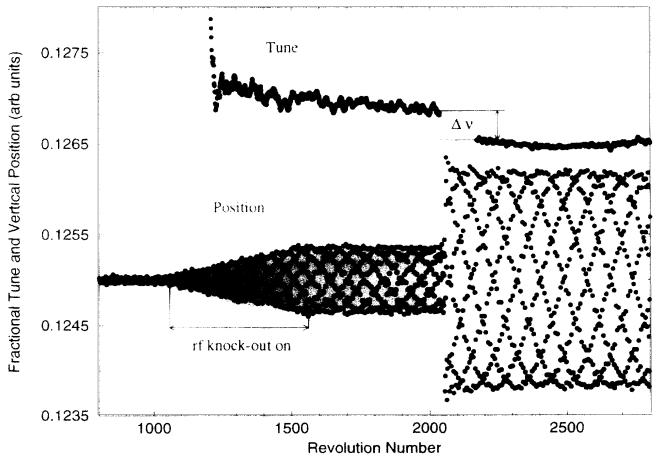

FIG. 4. Plot of both the measured vertical fractional tune ν_z and the position measurement at the first vertical BPM vs revolution number. This is a subsection of the same data displayed in Fig. 3. The change in tune near revolution 2000 results from the change in action I. The change in tune due to the change in action, of about 0.0003 was small compared to the tune change resulting from a power supply ripple of about 0.004

C. Fitting the nonlinear resonance strength

While the contours of constant H_2 can be used to determine resonance parameters, B, α_{11}, and δ_1 up to a scaling constant, there is, however, an interesting trick to obtain the absolute scaling factor by using the time derivative of the resonance phase $\dot{\phi}_1$. The resonance phase advance per turn $\Delta\phi_1$ can be obtained from the Hamilton's equation of motion by differentiating H_2 in Eq. (14), i.e.,

$$\frac{\Delta\phi_1}{2\pi} \approx \dot{\phi}_1 = \frac{\partial H_2}{\partial J_1} = \delta_1 + \alpha_{11} J_1 + 2^{1/2} B \left(-6 J_1^{1/2} + \frac{J_2}{J_1^{1/2}} \right) \cos\phi_1 . \tag{22}$$

Using δ_1, α_{11}, and B as adjustable parameters with the measured phase $\mu = \mu_m$ fixed at -2.13 rad (see Sec. III B), the phase advance per revolution $\Delta\phi_1$, was fit to Eq. (22). Some typical results are shown in Fig. 5. Here a 10-turn running average was used for both J_x and ϕ_1, so that the features of the nonlinear coupling resonance could be seen more clearly.

By fitting 25 different kicks, we found that the mean resonance strength was given by $B = (1.100 \pm 0.325)\ (\pi\mathrm{m})^{-1/2}$. Since the phase advance of ϕ_1 was not very sensitive to the value of α_{11}, the value of α_{11} was found instead by matching the curvature of the nonlinear coupling circle (see Sec. III D 1) to the experimental data when only a horizontal kick was applied. The effective nonlinear detuning was found to be $\alpha_{11} = (2100 \pm 300)\ (\pi\mathrm{m})^{-1}$.

D. Fitting the nonlinear Hamiltonian

Drawing contours of the constant Hamiltonian for the difference resonance of Eq. (14), in resonance phase space $(\sqrt{2\beta_x J_1}\cos\phi_1, \sqrt{2\beta_x J_1}\sin\phi_1)$, allows one to visualize the agreement between the measured data and theory. In this section, experimental data of the Poincaré surface of section will be compared with the Hamiltonian tori.

1. Horizontal kick

When only a horizontal kick was applied, Eq. (20) was used to draw both the launching circle and coupling arc. The data was inspected to find $J_2 \approx I_z + 2I_x$ while δ_1 was adjusted for each kick. It was necessary to adjust δ_1 for each kick because the base tunes were not constant. Three data sets with different values of J_2 are shown in Fig. 6. The curvature of the coupling circle was used to determine the value of α_{11} to be $\alpha_{11} = (2100 \pm 300)\ (\pi\mathrm{m})^{-1}$.

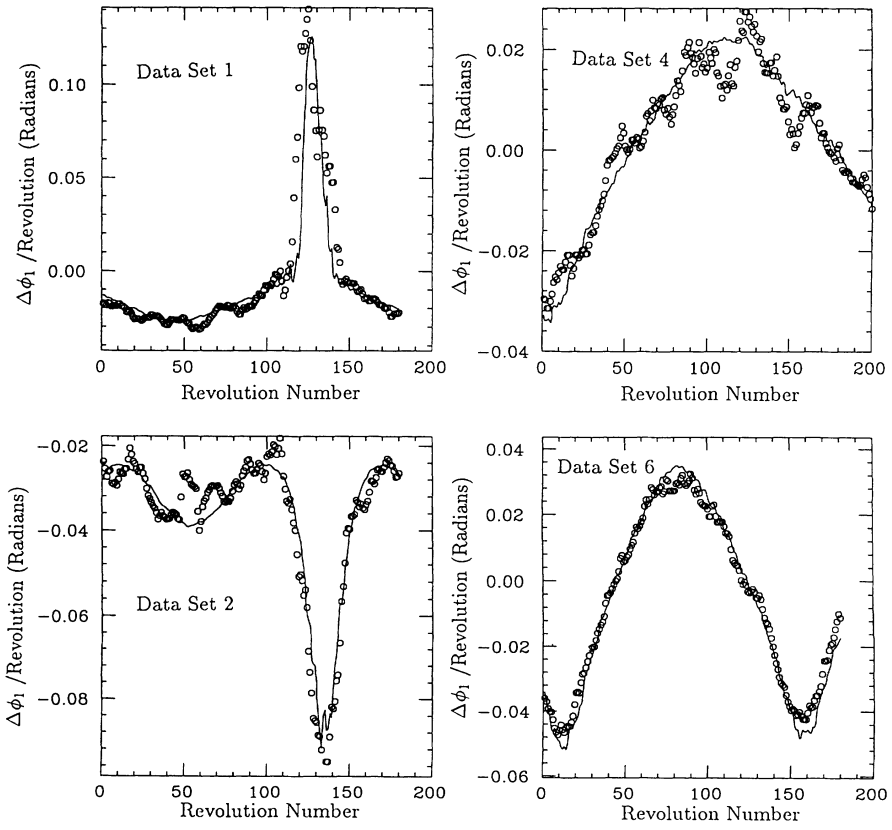

FIG. 5. Plot of measured (open circles) and predicted (solid lines) $\Delta\phi_1$ per revolution for 4 of the 6 data sets shown in Fig. 7.

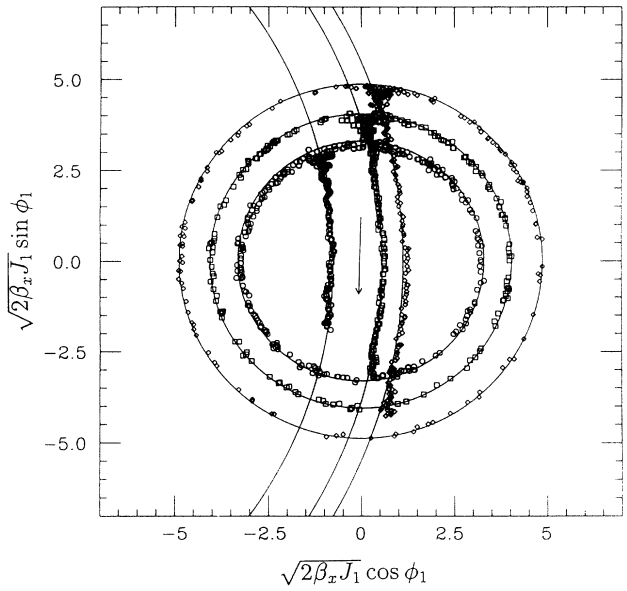

FIG. 6. The Poincaré surface of section plot of data (symbols) and fit (solid lines) to the Hamiltonian flow of Eq. (20) for three different values of J_2. There was no vertical kick and both the launching and coupling arcs are shown. The scales are in mm. The curvature of the coupling arcs was used to obtain $\alpha_{11} = (2100 \pm 300)\ (\pi\ \mathrm{m})^{-1}$.

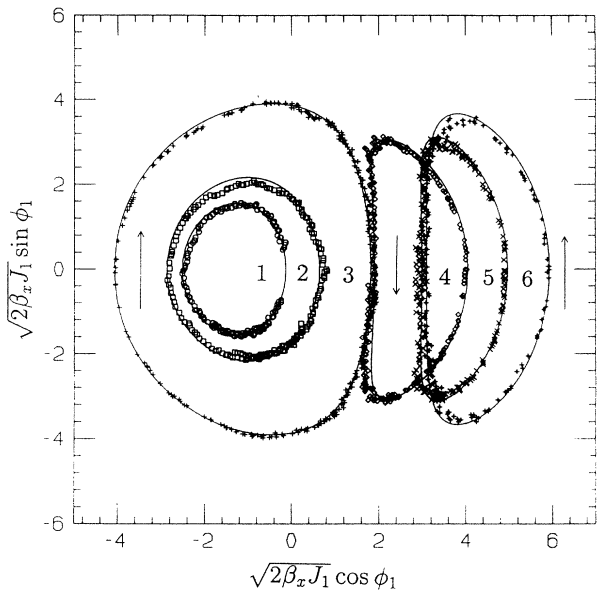

FIG. 7. The Poincaré surface of section plot of data (symbols) and fit (solid lines) to the tori of the Hamiltonian of Eq. (14). The vertical kick was held constant and the strength of the horizontal kick was varied. The scales are in mm. Because J_2 of all tori are different, the corresponding SFP also moves. Each torus in this figure can be enclosed by the corresponding launching and coupling circles with the appropriate δ_1 and J_2 values.

2. Both horizontal and vertical kicks

When there were both horizontal and vertical kicks, the data of the Poincaré maps in the resonance rotating frame were fit to the tori of the Hamiltonian of Eq. (14). The values of B, α_{11}, and μ_m were again held constant, while the value of δ_1 was adjusted for each kick. The value of J_2 used was the sum of the maximum of $2I_x$ and the minimum of I_z both of which were obtained from the data. The sharpness of the transition from the launching to the resonance circle is sensitive to the minimum value of I_z. By using the value of J_2 obtained by this prescription, the minimum value of I_z was not overestimated. The value of the constant $H_2 - [Q_z J_2 + \alpha_{zz} J_2^2/2]$ was determined by the requirement that $\cos\phi_1$ was equal to ± 1 when I_x was a maximum. Whether $\cos\phi_1$ was set to $+1$ or to -1 depended upon which side of the separatrix the beam bunch was on.

In Fig. 7, six data sets are shown for which the strength of the vertical kick was held constant while the strength of the horizontal kick was incremented. The tori of the Hamiltonian flow of Eq. (14), which fit these data, are also displayed as the solid lines in Fig. 7. The movement of the coupling circle from kick to kick is due to the modulation of the base tunes. For a constant kick amplitude, the resonance proximity parameter δ_1 was found to vary by about $\pm 2 \times 10^{-3}$, which is consistent with the expected tune modulation of the betatron tune due to a power supply ripple.

3. Slope of δ_1 vs J_2

A further prediction of the resonance Hamiltonian is that the value of δ_1 should depend upon J_2. From the definition of δ_1 in Eq. (14) it follows that

$$\frac{\partial \delta_1}{\partial J_2} = \alpha_{xz} - 2\alpha_{zz}. \tag{23}$$

The experimentally measured dependence of δ_1 on J_2 is shown in Fig. 8. From the slope of δ_1 vs J_2 the quantity $\alpha_{xz} - 2\alpha_{zz}$ was found to be $(-1278 \pm 150)\ (\pi\mathrm{m})^{-1}$. The zero intercept, $Q_x - 2Q_z + 6$, was about -5.0×10^{-4}.

4. Locking tunes on resonance

One additional prediction of this Hamiltonian analysis concerns the effect of the resonance strength on the betatron tunes. Depending on the initial values of J_1, J_2, and δ_1 two qualitatively different responses of the betatron tunes can be seen. If the contour of constant H_2 does not loop around the origin in resonance phase space then the time average of $\Delta\phi_1$, in Eq. (22), is zero. For these cases, shown as data sets 1, 4, 5, and 6 in Fig. 7, the time average of $\dot{\phi}_1$ is identically zero. One particular example of the betatron tunes locking to resonance harmonic is shown in the top half of Fig. 9 which plots $\dot{\phi}_1$ vs the revolution number for data set 6 in Fig. 7. Here, the tunes were measured by tracking the phase advance

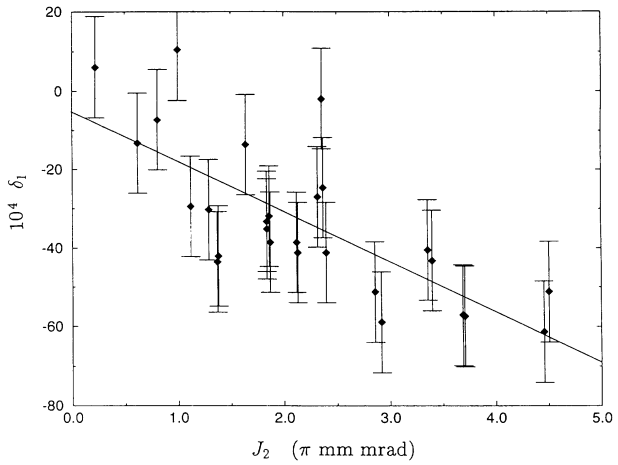

FIG. 8. Plot of δ_1 vs J_2. The large scatter is presumably due to the modulation of the base tunes.

as explained in Sec. III B 1. The bottom half of Fig. 9 displays the tune information for data set 3 in Fig. 7. It is worth noting that the tune, in the rotating reference frame, approaches zero for this data set as well. Tracking the beam centroid in the same phase space map as shown in Fig. 7, the "particle" is seen to cross over the separatrix and begin to rotate counterclockwise, after about 1700 revolutions, as was the case from the beginning for data set 6. It is not clear if this crossing of the separatrix was made possible by the base tune modulation in the cooler ring, which moved the location of the separatrix or if it was possible due to the time dependent terms in the Hamiltonian. This latter condition can only occur for orbits near the separatrix in chaotic motion.

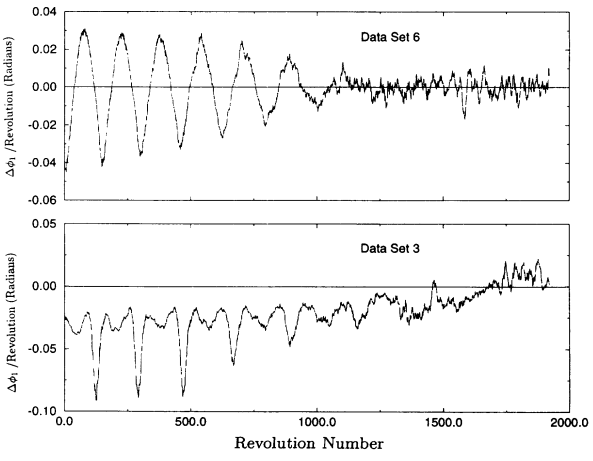

FIG. 9. Example of the betatron tunes "locking" to the resonance. The top plot shows the tune in resonance rotating frame for data set 6 in Fig 7. The bottom plot is for data set 3. The tunes were measured by tracking the phase of the particle in the resonance rotating phase space.

E. Effect of averaging

The Hamiltonian analysis presented here isolates the dominant resonance. However, it should be noted that the experimentally measurable conjugate variables were (I_y, ϕ_y), while the resonance Hamiltonian has been transformed to the conjugate coordinates (J_y, γ_y). The relationship between these coordinates is given in Eq. (8), which shows that for J_y to be approximately invariant, I_y must carry information of all nearby resonances. Recall that the resonance data, displayed in Figs. 5, 6, and 7, was filtered by using a 10-turn running average. While this averaging did serve to minimize the difference between the two sets of coordinates it is tempting to try to measure the time dependent fluctuations in the unfiltered data. In particular, it is clear from inspecting Eq. (4) that it should be possible to deduce the values of

$$\begin{aligned}
&\sum_m A_{30m}\cos(3\phi_x - m\theta + \alpha_{30m}),\\
&\sum_m B_{12m}\cos(\phi_x + 2\phi_z - m\theta + \beta_{12m}),\\
&\sum_m B_{10m}\cos(\phi_x - m\theta + \beta_{10m}),\\
&\sum_m B_{1-2m}\cos(\phi_x - 2\phi_z - m\theta + \beta_{1-2m}),
\end{aligned} \tag{24}$$

from the unfiltered data. This information might be useful in the implementation of a scheme to reduce the harmful effects of the nonlinearities.

The effort to deduce the parameters in Eq. (24) from the unfiltered data is complicated by nonlinearities in

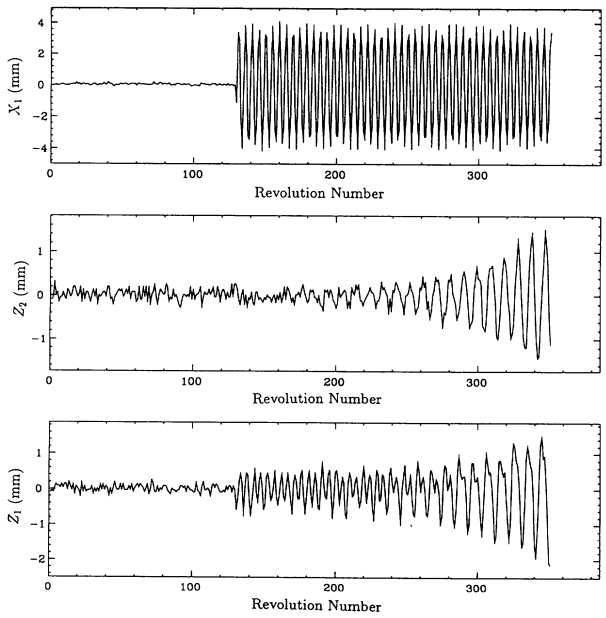

FIG. 10. Plot of position measurements, at each revolution, at x_1, z_1, and z_2. At the time of the initial horizontal kick the position measured in the first vertical BPM (bottom plot) begins to oscillate, at the horizontal tune. This is clearly evidence for a tilted vertical BPM.

the electronics, imperfect conversion to normalized coordinates, and coupling between the two planes of betatron motion.

Coupling between the two planes of motion in the measured data can result from resonant linear coupling [12], misalignment in the transverse kickers or misalignment in one of the BPM's. Evidence of misalignment in a vertical BPM can be seen in Fig. 10 which shows the position measurements in the vertical plane, at the time of a horizontal kick. The motion that appears in the first vertical BPM at the time of the kick, before significant motion is evident in the second vertical BPM, presumably results from a misalignment of that BPM. Due to the difficulty in accounting for and removing all the sources of systematic error in the measurements, it has not yet been possible to deduce unambiguously the amplitude and phase of the remaining time dependent terms in the Hamiltonian of Eq. (9).

IV. COMPARISON BETWEEN MEASURED AND CALCULATED PARAMETERS

A. Comparison of measured and calculated resonance strength

Since sextupoles drive the difference resonance it is possible to calculate the resonance strength from their known distribution. A simple computer program was written to evaluate B in Eq. (5) using the Courant-Snyder parameters obtained from the methodologic accelerator design (MAD) computer program with the same quadrupole values used during the experiment. Sextupole contributions included in the calculation of B were the 14 chromaticity correcting sextupoles which were energized during the run as well as the end sextupole fields of the 12 main dipole magnets. The strength of the sextupole contribution at the end of each dipole magnet was deduced previously [8] from the measured chromaticities C_x and C_z. The calculated resonance strength was found to be 2.93 $(\pi\mathrm{m})^{-1/2}$. This calculated value of the resonance strength is larger than the measured value by a factor of about 2.7. The reason for this discrepancy presumably lies with the relatively poor linear optics modeling of the cooler ring. The measured and calculated tunes are in good agreement but this masks the fact that the measured and calculated β functions often differ by as much as a factor of 2. It should be kept in mind that while the particle motion is in resonance with the Q_x-2Q_z+6 harmonic, the resonance strength contributed by individual sextupoles do not generally add coherently. It is not surprising that the measured resonance strength was somewhat smaller than the calculated value. When setting up for the experiment, individual sextupoles were adjusted to maximize the beat period of energy exchange between the x and z planes of oscillation. For a given δ_1 and J_1, $\dot{\phi}_1$ is proportional to the resonance strength Eq. (22), thus, maximizing the beat period served to minimize the resonance strength.

B. Comparison of the measured and calculated resonance phase

Some care needs to be taken concerning the relationship between the phase factor measured in our experiment μ_m, which was added to the measurement of ϕ_1 so that the oscillation occurred about $\phi_1 = 0$, and the phase factor $\mu = \beta_{1-2-6}$ calculated from Eq. (5). Recall that $\phi_1 \approx \phi_x - 2\phi_z + 6\theta + \mu$, where γ_y has been approximated by ϕ_y, which simply ignores the high frequency fluctuations. With this approximation, it is easy to show that $\phi_1 = \phi_{xo} - 2\phi_{zo} + \mu$, where ϕ_{yo} are the betatron phases of the bunch at $\theta = 0$. Since the measured phases, ϕ_{ym}, in this approximation, are given by $\phi_{ym} = \phi_{yo} + \int_o^{s(y)} \frac{ds}{\beta_y}$, where $s(y)$ is the location at which the measurement was made, it follows that the measured phase angle μ_m should be given by

$$\mu_m = \int_o^{s(x)} \frac{ds}{\beta_x} - 2\int_o^{s(z)} \frac{ds}{\beta_z} + \mu. \tag{25}$$

Using the calculated value of β_{1-2-6} from Eq. (5) of -2.43 rad together with the phase advances in each plane of oscillation obtained from MAD, μ_m was found using Eq. (25) to be -2.53 rad, which agrees well with the measured resonance phase of -2.13 rad. The determination of whether this rather good agreement was due to coincidence or accurate modeling of the nonlinearities in the cooler ring must await a more refined linear optics model.

C. Comparison of the detuning parameters

Comparison of the detuning parameters is more difficult than comparison of either the resonance strength or the phase factor. This is because sextupoles, as explained in Appendix A, contribute to tune shifts with action only in second order and possible contribution to the detuning parameters from octupole fields have not been included. Until the linear optics of the cooler ring are accurately modeled, and the octupole fields accounted for, it is not expected that there will be good agreement between calculated and measured detuning parameters.

V. CONCLUSION

The betatron difference resonance, $Q_x - 2Q_z = -6$, was investigated at the IUCF cooler ring. It was found that a single resonance Hamiltonian can accurately describe the coupled motion. The complicated motion in the 4D phase space can be reduced to invariant tori in the resonance rotating frame. It was possible to match both the phase advance per turn of ϕ_1 and the contour traced in the map of $(\sqrt{2\beta_x J_1}\cos\phi_1, \sqrt{2\beta_x J_1}\sin\phi_1)$ with the predictions from the Hamiltonian Eq. (12). We have developed a systematic method for deducing the resonance Hamiltonian from particle motion near a 2D resonance. Such measurements are important for improving the performance of high brightness storage rings.

The resonance strength B and phase factor μ are compared with the calculated values. As our understanding

of both the linear optics and cooler ring nonlinearities improves, the performance of the cooler ring will be enhanced. We have pointed out some of the difficulties, such as tune modulation and BPM misalignment, in nonlinear experiments. Extreme care is needed to achieve the goal of understanding nonlinearities in synchrotrons.

ACKNOWLEDGMENTS

Work supported in part by grants from the National Science Foundation NSF Grant No. PHY-9221402 and from the U.S. Department of Energy Grant No. DE-FG02-93ER40801

APPENDIX A: NONLINEAR DETUNING

The A_{ij} in Eq. (9) are given by

$$\begin{aligned}
A_{xx} &= 24\frac{\partial\sum_a}{\partial\phi_x}\sum_m[A_{30m}\cos(3\phi_x - m\theta + \alpha_{30m}) + 3A_{10m}\cos(\phi_x - m\theta + \alpha_{10m})],\\
A_{xz} &= -12\frac{\partial\sum_a}{\partial\phi_x}\sum_m[A_{30m}\cos(3\phi_x - m\theta + \alpha_{10m}) - \left(4\frac{\partial\sum_a}{\partial\phi_x} - 8\frac{\partial\sum_a}{\partial\phi_z}\right)\sum_m[B_{12m}\cos(\phi_x + 2\phi_z - m\theta + \beta_{12m})\\
&\quad +2B_{1-2m}\cos(\phi_x - 2\phi_z - m\theta + \beta_{1-2m}) + 4B_{10m}\cos(\phi_x - m\theta + \beta_{10m})],\\
A_{zz} &= +8\frac{\partial\sum_b}{\partial\phi_x}\sum_m[B_{12m}\cos(\phi_x + 2\phi_z - m\theta + \beta_{12m})\\
&\quad +2B_{1-2m}\cos(\phi_x - 2\phi_z - m\theta + \beta_{1-2m}) + 4B_{10m}\cos(\phi_x - m\theta + \beta_{10m})].
\end{aligned} \tag{A1}$$

The nonlinear detuning parameters α_{ij} can now be found by averaging the A_{ij} over one revolution of the accelerator:

$$\begin{aligned}
\alpha_{xx} &= -36\sum_m\left[\frac{A_{30m}^2}{3Q_x - m} + \frac{3A_{10m}^2}{Q_x - m}\right],\\
\alpha_{xz} &= 8\sum_m\left[\frac{6A_{10m}B_{10m}}{Q_x - m}\cos(\alpha_{10m} - \beta_{10m}) - \frac{B_{12m}^2}{Q_x + 2Q_z - m} + \frac{B_{1-2m}^2}{Q_x - 2Q_z - m}\right],\\
\alpha_{zz} &= -4\sum_m\left[\frac{B_{12m}^2}{Q_x + 2Q_z - m} + \frac{B_{1-2m}^2}{Q_x - 2Q_z - m} + \frac{4B_{10m}^2}{Q_x - m}\right].
\end{aligned} \tag{A2}$$

The sum over m contains all integers except those for which the betatron tunes are close to a resonance condition.

APPENDIX B: THE PARAMETRIC DEPENDENCE OF RESONANCE CONDITION

The Hamiltonian (14) depends only on two parameters,

$$d = 4\frac{\delta_1}{\alpha_{11}J_2}, \quad b = 8\frac{B}{\alpha_{11}\sqrt{J_2}}, \tag{B1}$$

where d and b signify, respectively, the effective proximity parameter to the resonance line and the effective resonance strength for particles with an identical J_2. Defining the normalized phase space coordinates as

$$(\xi,\eta) = \left(\sqrt{\frac{2J_1}{J_2}}\cos\phi_1, \sqrt{\frac{2J_1}{J_2}}\sin\phi_1\right), \tag{B2}$$

the launching and the coupling circles are, respectively, given by

$$\xi^2 + \eta^2 = 1, \quad (\xi - b)^2 + \eta^2 = (b^2 - d - 1). \tag{B3}$$

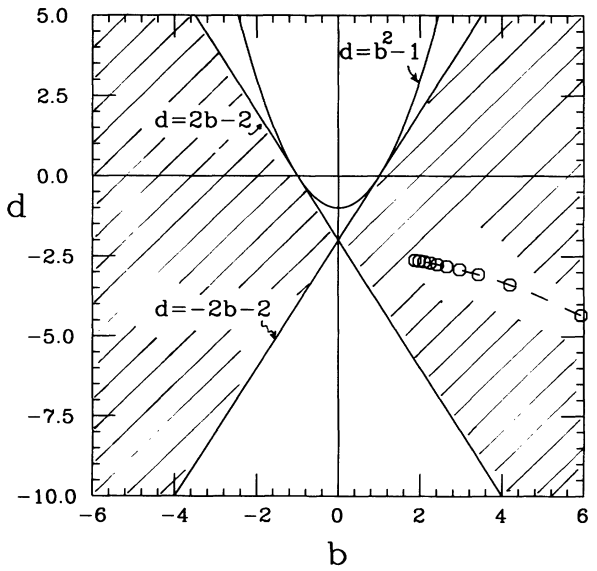

FIG. 11. The parametric dependence of the fixed points bifurcation for the 2D resonance Hamiltonian. The UFP's of Eq. (19) exist in the shaded region. The coupling circle exists when $d \le b^2 - 1$. The circle symbols are parametric conditions of the experimental data presented in Sec. III.

Here, the radius of the launching circle is one, and the coupling circle exists only when $d \leq b^2 - 1$. Thus the resonance bifurcation occurs at $d = b^2 - 1$, shown as the parabolic curve in Fig. 11. Now, the condition for the coupling circle to intercept the ξ axis within the launching circle is given by

$$\begin{array}{l} d - 2b \leq -2 \text{ and } d + 2b \geq -2 \text{ if } b \geq 0 \\ d - 2b \geq -2 \text{ and } d + 2b \leq -2 \text{ if } b < 0, \end{array} \tag{B4}$$

shown as shaded area bounded by two straight lines in Fig. 11. Particles, which satisfy the condition (B4), are strongly perturbed by the coupling resonance. The bifurcation of the UFP's of Eq. (19) occurs at $d \pm 2b = -2$. The circle symbols shown in Fig. 11 correspond to experimental conditions discussed in Sec. III.

In the limit of a small detuning parameter α_{11}, the system depends on a single parameter $d/2b$. The coupling circle becomes a vertical line in the phase space of the resonance rotating frame. In the parametric range $d/2b \in [-1, 1]$, the resonance line intersects the launching circle. Thus the bifurcation of the UFP's of Eq. (19) occurs at $d/2b = \pm 1$.

To evaluate the effect of the resonance on the particle motion of a beam, one can plot the parametric distribution of the beam on Fig. 11. Particles lying inside the shaded area will be affected strongly by the coupling resonance.

[1] A.J. Dragt, in *Physics of High Energy Particle Accelerators*, Published Lectures from the Summer School on High Energy Particle Accelerators, edited by R.A. Carrigan, F.R. Hudson, and M. Month, AIP Conf. Proc. No. 87 (AIP, New York, 1982), p. 147; A.J. Dragt *et al.*, Ann. Rev. Nucl. Sci. **38**, 455 (1992).

[2] G. Guignard, CERN Report No. 76-06, 1976 (unpublished); CERN Report No. 78-11, 1978 (unpublished); A. Schoch, CERN Report No. 57-21, 1958 (unpublished).

[3] L. Michelotti, in *Physics of Particle Accelerators*, Proceedings of the Fifth Annual U.S. Particle Accelerator School, edited by M. Month and Margaret Deines, AIP Conf. Proc. No. 153 (AIP, New York, 1987), p. 236; R. Ruth, in *Nonlinear Dynamics of Particle Accelerators*, edited by J.M. Jowett, M. Month, and S. Turner, Lecture Notes in Physics Vol. 247 (Springer-Verlag, New York, 1985), p. 37; W.E. Gabella, R. Ruth, and R.L. Warnock, Phys. Rev A **46**, 3493 (1992).

[4] M. Berz, Part. Accel. **24**, 109 (1989).

[5] E. Forest, L. Michelotti, A.J. Dragt, and J.S. Berg, in *Stability of Particle Motion in Storage Rings, Proceedings of the Particles and Fields Series 54*, edited by M. Month, A.G. Ruggiero, and W.T. Weng, AIP Conf. Proc. No. 292 (AIP, New York, 1992), p. 418.

[6] P.L. Morton *et al.*, IEEE Trans. Nucl. Sci. **32**, 2291 (1985); M. Cornacchia and L. Evans, Part. Accel. **19**, 125 (1986); D.A. Edwards, R.P. Johnson, and F. Willeke, *ibid.* **19**, 145 (1986); A. Chao *et al.*, Phys. Rev. Lett. **61**, 2752 (1988); L. Evans *et al.*, in *Proceedings of the European Particle Accelerator Conference, Rome*, 1988, edited by S. Tezzari and K. Huebner (World Scientific, Teaneck, N.J., 1989), p. 618.

[7] S.Y. Lee *et al.*, Phys. Rev. Lett. **67**, 3768 (1991).

[8] D.D. Caussyn *et al.*, Phys. Rev. A **46**, 7942 (1992).

[9] M. Ellison *et al.*, in *Stability of Particle Motion in Storage Rings* (Ref. 5), p. 170.

[10] J.Y. Liu, Part. Accel. **41**, 1 (1993).

[11] R.E. Pollock, Annu. Rev. of Nucl. Part. Sci. **41**, 357 (1991).

[12] J.Y. Liu *et al.*, Phys. Rev. E **49**, 2347 (1994).

[13] E.D. Courant and H.S. Snyder, Ann. Phys. **3**, 1 (1958).